


Article

# Tungsten-Based Mesoporous Silicates W-MMM-E as Heterogeneous Catalysts for Liquid-Phase Oxidations with Aqueous H<sub>2</sub>O<sub>2</sub>

Nataliya Maksimchuk <sup>1,2,\*</sup>, Irina Ivanchikova <sup>1</sup>, Olga Zalomaeva <sup>1</sup>, Yurii Chesalov <sup>1,2</sup>,  
Alexandr Shmakov <sup>1,2</sup> , Vladimir Zaikovskii <sup>1,2</sup> and Oxana Kholdeeva <sup>1,2,\*</sup>

<sup>1</sup> Borekov Institute of Catalysis, Lavrentieva Ave. 5, Novosibirsk 630090, Russia; idi@catalysis.ru (I.I.); zalomaeva@catalysis.ru (O.Z.); chesalov@catalysis.ru (Y.C.); shurka@catalysis.ru (A.S.); vis@catalysis.ru (V.Z.)

<sup>2</sup> Department of Natural Sciences, Novosibirsk State University, Pirogova Str. 2, Novosibirsk 630090, Russia

\* Correspondence: nvmax@catalysis.ru (N.M.); khold@catalysis.ru (O.K.); Tel.: +7-383-326-9433 (N.M. & O.K.)

Received: 10 January 2018; Accepted: 18 February 2018; Published: 27 February 2018

**Abstract:** Mesoporous tungsten-silicates, W-MMM-E, have been prepared following evaporation-induced self-assembly methodology and characterized by elemental analysis, XRD, N<sub>2</sub> adsorption, STEM-HAADF (high angle annular dark field in scanning-TEM mode), DRS UV-vis, and Raman techniques. DRS UV-vis showed the presence of two types of tungsten oxo-species in W-MMM-E samples: isolated tetrahedrally and oligomeric octahedrally coordinated ones, with the ratio depending on the content of tungsten in the catalyst. Materials with lower W loading have a higher contribution from isolated species, regardless of the preparation method. W-MMM-E catalyzes selectively oxidize of a range of alkenes and organic sulfides, including bulky terpene or thianthrene molecules, using green aqueous H<sub>2</sub>O<sub>2</sub>. The selectivity of corresponding epoxides reached 85–99% in up to 80% alkene conversions, while sulfoxides formed with 84–90% selectivity in almost complete sulfide conversions and a 90–100% H<sub>2</sub>O<sub>2</sub> utilization efficiency. The true heterogeneity of catalysis over W-MMM-E was proved by hot filtration tests. Leaching of inactive W species depended on the reaction conditions and initial W loading in the catalyst. After optimization of the catalyst system, it did not exceed 20 ppm and 3 ppm for epoxidation and sulfoxidation reactions, respectively. Elaborated catalysts could be easily retrieved by filtration and reused several times with maintenance of the catalytic behavior.

**Keywords:** alkene; epoxidation; evaporation-induced self-assembly; heterogeneous catalysis; hydrogen peroxide; mesoporous tungsten-silicate

## 1. Introduction

Tungsten is catalytically very active and is used in the formation of diverse compounds as a catalyst in a wide range of chemical processes including H<sub>2</sub>O<sub>2</sub>-mediated oxidation [1–12]. However, attempts to design heterogeneous tungsten-based catalysts with sufficient stability under turnover conditions of liquid-phase oxidation with H<sub>2</sub>O<sub>2</sub> have been rather unsuccessful, as yet. Tungsten incorporation into already-synthesized supports could be achieved by either impregnation or grafting of tungsten species [13–18]. Direct incorporation involves adding the metal precursors to the synthesis mixture used to prepare the support. However, incorporation of tungsten into mesoporous silicates is not a trivial task since tungsten is considerably larger than silicon, with an ionic radius of 0.42 Å, compared to 0.26 Å [19]. Thus, tungsten-containing mesoporous molecular sieves usually have a serious drawback of the active metal leaching under turnover conditions of liquid-phase oxidation [20–24]. Numerous efforts have been focused on synthesizing materials in which the active

tungsten species are well isolated and anchored on the support through W–O–Si covalent bonds. In recent years, tungsten has been incorporated into high surface area mesoporous molecular sieves, such as MCM-41 [21,25–31], MCM-48 [32,33], SBA-15 [34–36], SBA-16 [23], HMS [37,38], MCF [39,40], KIT-5 [41], KIT-6 [24,42], and TUD-1 [43].

Successful incorporation of tungsten ions into the framework of a silicate network is a challenge in acidic medium because of formation of oligo-/polymeric non-peroxidic species [44,45]. Tungsten could be incorporated in the tetrahedrally coordinated positions of the MCM-41 framework in acidic medium when the Si/W ratio is  $\geq 30$  (i.e., 5.6 wt % of W or less) [26,28,29,37]. The higher W content resulted in the formation of extra-framework crystalline  $\text{WO}_3$ , as detected by XRD and Raman spectroscopy. To improve the dispersion of tungsten oxide species in the silicate matrix, an oxoperoxo route was developed by Brégeault et al. [21,25]. Indeed, excess  $\text{H}_2\text{O}_2$  generated low condensed oxoperoxometalate species in the gel, thus avoiding formation of extra-framework crystalline  $\text{WO}_3$  during calcination [46]. However, the leaching of active species under turnover conditions was not avoided and up to 55% of the initial tungsten content was leached into solution during the catalytic reaction [25].

Another possibility for improving tungsten dispersion within a silicate matrix was reported to be through synthesis in basic medium (pH > 8) where monomeric tungsten species, e.g.,  $[\text{WO}_4]^{2-}$ , are predominant [31,46]. One more approach was suggested by Gao et al. [39]. A range of  $\text{WO}_3$ -MCF samples were synthesized via hydrothermal synthesis, followed by calcination and treatment with 1 M of ammonium acetate (80 °C, 6 h) to remove crystalline  $\text{WO}_3$  species [39]. Thus, obtained materials contained 0.3–0.5 wt % of tungsten in the form of isolated  $[\text{WO}_4]^{2-}$  tetrahedral species and were not susceptible to leaching.

Tungsten-based W-SBA-16 [23], W-KIT-5 [41] and W-KIT-6 [42] materials, obtained by hydrothermal synthesis under acidic conditions, contained framework  $[\text{WO}_4]^{2-}$  tetrahedral species and octahedrally coordinated polytungstate at low W loadings. However, these materials suffered from tungsten leaching under turnover conditions of catalytic oxidation with aqueous  $\text{H}_2\text{O}_2$  [23,41,42]. In the case of W-KIT-5, up to 75% of the active metal had leached out from the catalyst, according to ICP-OES analysis of the spent reaction mixture [41]. Substantial leaching of W species was also observed during a blank experiment on the treatment of the catalyst with  $\text{H}_2\text{O}_2$  without substrate.

Recently, we reported the successful application of the affordable and versatile evaporation-induced self-assembly (EISA) approach for the preparation of mesoporous hydrothermally stable and leaching tolerant titanium- [47] and niobium-silicates [48], designated as Ti- and Nb-MMM-E (MMM = mesoporous mesophase material, E stands for EISA), using tetraethyl orthosilicate (TEOS) as the silica precursor and cetyltrimethylammonium bromide (CTAB) as the templating agent. Employment of acetylacetone (acac) as the chelating agent for stabilization of metal precursors in the synthesis prevented  $\text{TiO}_2$  or  $\text{Nb}_2\text{O}_5$  precipitation and assisted in the generation of active centers that were well-dispersed within the silica matrix. Recently, Subramaniam and co-workers employed EISA to synthesize zirconium- [49], tungsten- [50], and molybdenum-containing [51] mesostructured silicates using TEOS as the silica precursor, Pluronic P123 as the templating agent and  $\text{ZrOCl}_2 \cdot 8\text{H}_2\text{O}$ ,  $\text{WCl}_6$  or  $\text{MoCl}_5$  as metal sources. Highly dispersed tungsten species (isolated tetrahedral  $[\text{WO}_4]^{2-}$  along with octahedral polytungsten species) were generated at W loadings of 2.9–13.8 wt %, while at the higher loading (22.2 wt % W),  $\text{WO}_3$  nanocrystallites were also formed [50]. Thus, obtained W-EISA materials were examined during the gas-phase reaction of ethylene and 2-butene metathesis to form propene (450 °C, 1 atm). However, no liquid-phase oxidation was reported, most likely because of leaching problems.

The aim of our work was to develop an EISA-based synthetic protocol for the preparation of leaching-tolerant mesoporous tungsten-silicates, which could be employed as heterogeneous catalysts for liquid-phase oxidation. Here, we report a versatile procedure for the synthesis of materials designated as W-MMM-E, containing 0.8–1.6 wt % of W and using either tungsten(VI) ethoxide modified with acetylacetone or  $\text{WO}_2(\text{acac})_2$  as the tungsten precursor. We also report their characterization and evaluation

during H<sub>2</sub>O<sub>2</sub>-based selective oxidation of various alkenes and organic sulfides. The catalyst's stability toward tungsten leaching and reusability was the main focus of this study.

## 2. Results and Discussion

### 2.1. Catalyst Synthesis and Characterization

Acetylacetonone has been widely employed as a hydrolysis-retarding dopant in sol-gel and template syntheses of mesoporous metal-silicates [20,52]. Use of this chelating agent in the synthesis of Ti-MMM-E catalysts by EISA not only prevented TiO<sub>2</sub> precipitation but also assisted in the generation of specific di(oligo)meric Ti centers within the silica matrix [48]. The same acac chelating ligand was successfully employed for stabilization of Nb precursors in the synthesis of Nb-MMM-E materials using the same EISA methodology [48]. The formation of oxo alkoxide/acac WO(OR)<sub>x</sub>(acac)<sub>y</sub> complexes by the interaction of W oxo alkoxides with acac was addressed in the literature [53,54]. All of these prompted us to use acac in the synthesis of W-MMM-E materials.

Method A (see Section 3) was, therefore, similar to the procedure reported earlier for the synthesis of Ti-MMM-E [47] and Nb-MMM-E [48] materials. Tungsten(VI) ethoxide modified with acetylacetonone was taken as the W precursor. The molar ratios of W/Si were 0.18/50 and 0.35/50 (samples A-1 and A-2, respectively).

In Methods B and C, we used WO<sub>2</sub>(acac)<sub>2</sub> as the tungsten precursor, which was synthesized and characterized beforehand. In Method B, we also attempted to prevent hydrolysis and oligomerization of tungsten species by eliminating water content in the reaction mixture, i.e., using dry ethanol instead of 95% and excluding HCl. According to the EISA methodology, the introduction of tungsten into the final material was almost quantitative (except for samples A due to poor solubility of tungsten ethoxide), as confirmed by the elemental analysis data (Table 1).

**Table 1.** Physicochemical properties of W-MMM-E catalysts.

Catalyst	Si/W <sup>a</sup>	W <sub>calc</sub> <sup>b</sup> , wt %	W <sub>exp</sub> <sup>c</sup> , wt %	S <sub>BET</sub> , m <sup>2</sup> /g	V <sub>p</sub> <sup>d</sup> , cm <sup>3</sup> /g	D <sub>p</sub> <sup>e</sup> , nm
A-1	278	1.0	0.9	1130	0.57	2.48
				1180 <sup>f</sup>	0.50	2.49 <sup>f</sup>
A-2	143	2.0	1.6	1440	0.61	2.51
B-1	294	1.0	0.9	1240	0.51	2.54
B-1.4	208	1.4	1.4	1140	0.49	2.56
C-1	294	1.0	0.8	1170	0.46	2.41
				1180 <sup>f</sup>	0.49	2.45 <sup>f</sup>

<sup>a</sup> Molar ratio used in the synthesis; <sup>b</sup> Calculated based on the Si/W molar ratio used in the synthesis; <sup>c</sup> Based on elemental analysis data for calcined samples; <sup>d</sup> Mesopore volume; <sup>e</sup> Mean pore diameter; <sup>f</sup> After catalyst reuse in cyclooctene oxidation (reaction conditions were as in Table 2, 50% H<sub>2</sub>O<sub>2</sub>); samples were calcined before measurements.

The small angle XRD patterns of W-MMM-E samples, shown in Figure 1, exhibit a broad diffraction reflex around 3.0° (2θ). This indicates a long-range structural order of cylindrical mesopores, which is typical for silicate materials prepared by EISA [47,48,50]. The lattice constant, calculated using the XRD (10) reflection position for W-MMM-E, is close to that reported for Ti-MMM-E (5.0 vs. 5.2 nm) [47]. Moreover, the lack of any additional reflexes at higher 2θ values (Figure S1), except for the broad one corresponding to amorphous silicate, indicates the absence of crystalline WO<sub>3</sub>.

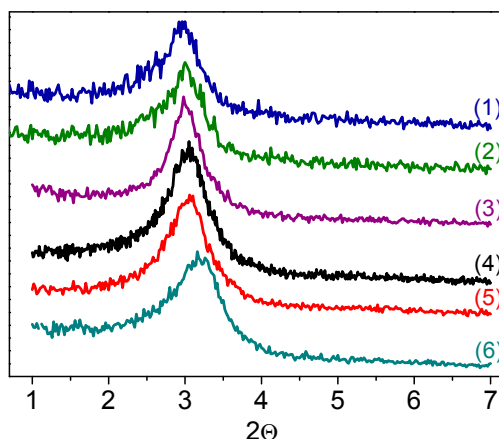


**Figure 1.** XRD patterns of calcined W-MMM-E catalysts: (1) C-1; (2) B-1.4; (3) A-1; (4) A-2; (5) A-2 after treatment with aqueous H<sub>2</sub>O<sub>2</sub> in CH<sub>3</sub>CN (25 °C, 1 h) and (6) A-2 after treatment with boiled water for 6 h.

The textural properties of all W-MMM-E samples measured by low-temperature nitrogen adsorption are presented in Table 1. All the solids possessed only mesopores and no micropores. Interestingly, the mean pore diameter for W-MMM-E is slightly less than that of Ti- and Nb-MMM-E materials (2.4–2.6 vs. 2.9–3.2 nm), while the silicate wall is oppositely thicker (2.5 vs. 2.2 nm). Texture parameters depend a little on the W precursor used. Both specific BET surface area and pore volume were slightly bigger for material A prepared via modification of tungsten ethoxide than for samples B and C synthesized using isolated WO<sub>2</sub>(acac)<sub>2</sub> complex (1330 m<sup>2</sup>/g and 0.57 cm<sup>3</sup>/g for A-1, versus 1170–1240 m<sup>2</sup>/g and 0.46–0.51 cm<sup>3</sup>/g for C-1 and B-1). Variations in the Si/W ratio produced very little effect on the texture parameter of the materials.

The DR UV-vis spectra of the W-MMM-E catalysts are shown in Figure 2.

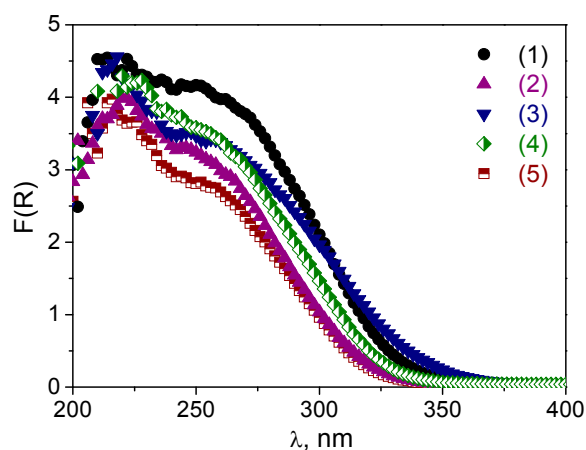


**Figure 2.** DR UV-vis spectra of calcined W-MMM-E catalysts: (1) A-2; (2) A-1; (3) B-1.4; (4) B-1; and (5) C-1.

All materials exhibit two main absorptions—a sharp band with a maximum centered at ca. 220–225 nm and a broad one at 250–255 nm. The adsorption peak at 230 nm is attributed to isolated tetrahedral [WO<sub>4</sub>]<sup>2−</sup> species because the spectrum of Na<sub>2</sub>WO<sub>4</sub> has a spinel structure [21,23]. Broad absorptions around 240–290 nm are typically assigned to octahedrally coordinated small oligomeric tungsten oxide species [23,31,32,41]. Thus, we may assume the presence of two types of tungsten oxo species in the W-MMM-E samples: isolated tetrahedrally coordinated and oligomeric octahedrally coordinated ones. The lower content of tungsten in the sample indicates a higher contribution of isolated

species. A shoulder at 310–320 nm in the spectra of samples with a higher amount of W (**A-2** and **B-1.4**) may indicate the presence of octahedrally coordinated polytungstate species or formation of  $\text{WO}_3$ -like nano-aggregates [41]. Importantly, for all the elaborated W-MMM-E materials, no adsorptions were detected around 380–450 nm, indicating the absence of crystalline  $\text{WO}_3$  on the catalyst surface [21,23,25,33,39,42,43]. As opposed to other known tungsten-silicates with close W loading ( $\text{Si}/\text{W} \geq 122$ ), i.e., W-MCM-48 [32,33] or  $\text{WO}_3$ -MCF [39], the EISA methodology enables better isolation of tungsten in the silicate matrix and prevents formation of  $\text{WO}_3$  agglomerates.

Raman spectroscopy was also employed to explore further the nature of the W species formed on the surface of the catalyst. The spectra of samples **A-1** and **A-2** are shown in Figure 3, in comparison with the spectra of bulk  $\text{WO}_3$  and tungsten-free silicate matrix. In spite of the distinction in the DRS-UV spectra, the Raman spectra of these samples were quite similar. The Raman spectrum of crystalline  $\text{WO}_3$  is characterized by strong bands at 808 and 720  $\text{cm}^{-1}$  along with peaks at 324 and 272  $\text{cm}^{-1}$  (Figure 3, curve (1)) [33,43,55,56]. Significantly, these peaks are absent in the Raman spectra of the W-MMM-E catalysts, corroborating the absence of  $\text{WO}_3$  crystallites and incorporation of well dispersed tungsten oxide species into the silica matrix. The spectra of W-MMM-E samples (Figure 3, curves (3) and (4)) are very similar to those of the pure EISA silica (Figure 3, curve (2)) except for the intense band at 975  $\text{cm}^{-1}$  which may be attributed to vibrations of the terminal W=O bonds [55,57,58]. Raman features between 1000 and 900  $\text{cm}^{-1}$  are typically observed in mono- and polytungstate species [22,41,57,58].

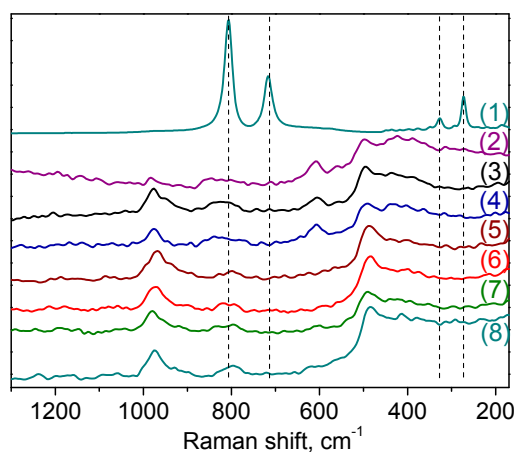


**Figure 3.** Raman spectra of (1)  $\text{WO}_3$ ; (2) calcined  $\text{SiO}_2$ -EISA matrix, and calcined W-MMM-E catalysts: (3) **A-2**; (4) **A-1**; (5) **A-2** after treatment with  $\text{H}_2\text{O}_2$ ; (6) **A-1** after treatment with  $\text{H}_2\text{O}_2$ ; (7) **A-2** after catalytic oxidation of cyclooctene; and (8) **A-1** after catalytic oxidation of cyclooctene. Reaction conditions were as in Table 2.

STEM-HAADF (high angle annular dark field in scanning-TEM mode) images of the W-MMM-E (sample **A-1**) exhibit nanoscale inclusions of tungsten associates, unevenly distributed over the silica surface. Two representative images are given in Figure 4. Figure 4a shows a piece of the catalyst with W-containing particles of 1–2 nm dispersed on the surface. However, such large particles are much less common in other parts of the catalyst. Some ordering of the mesopores with a periodicity of  $\sim 2$  nm can be noticed in Figure 4b. One can also distinguish here bright clusters with a size less than 1 nm and spots of particles with an elongated shape, which correspond to polytungstate species. These spots have a lower contrast, most likely because they are located inside the mesopores and not on the external surface of the catalyst particles.



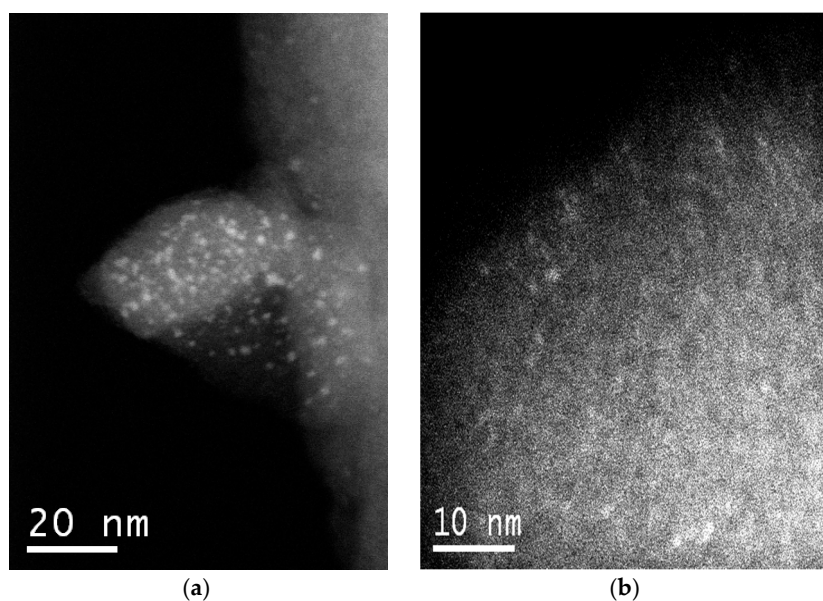


**Figure 4.** STEM-HAADF images of calcined **A-1** catalyst with different magnification.

## 2.2. Hydrothermal Stability and Stability towards $H_2O_2$

Hydrothermal stability is essential for the catalysts applied for oxidation using aqueous hydrogen peroxide. However, as has already been mentioned, tungsten-containing mesoporous silicates usually suffer from active metal leaching under turnover conditions during liquid-phase oxidation.

The stability of all the elaborated W-MMM-E samples was examined by treatments: (i) with boiling water for 6 h and (ii) with 0.11 M solution of  $H_2O_2$  in  $CH_3CN$  for 1 h at room temperature. Similar tests were previously employed for Ti-MMM-E [47] and Nb-MMM-E [48] materials. Figure 1 (curves (5) and (6)) shows the XRD patterns of sample **A-2** after the treatments. Both the position and width of the diffraction reflexes are very close, which suggests fairly good structural stability in the W-MMM-E solids synthesized by the EISA technique. Raman spectra also did not show changes after treatment with  $H_2O_2$  (Figure 3, compare curves (3), (4) and (5), (6)).

The DR UV-vis spectra after the treatments are given in Figure 5 along with Figures S2 and S3 in Supplementary Materials. One can see that, after the boiling procedure, the shoulder assigned to oligomeric tungsten oxo species (240–290 nm) decreased dramatically, and treated samples contained mostly isolated W. This effect was most pronounced for the A and B samples. Obviously, leaching of oligomeric W species occurred during the treatment, which was also confirmed by elemental analysis (Table S1): 19–107 ppm of leached W was detected in the reaction mixture after the catalyst was separated by filtration. The A materials were also not stable during the treatment with  $H_2O_2$ . Figure S2 showed a decrease in the shoulder at 240–290 nm in DR-UV spectra for both **A-1** and **A-2** samples, but it occurred less dramatically than in the case of the boiling procedure. On the other hand, the spectra of both **B-1** and **B-1.4** samples almost did not change (Figures S2 and S3, and Figure 5a). For sample **C-1**, both treatments caused a long-wave shift in the absorption band that was manifested to a greater extent in the case of the boiling procedure than following treatment with  $H_2O_2$  (Figure 5b). This shift may indicate some further agglomeration of the tungsten species. Thus, one may conclude that materials **B** and **C**, synthesized using the  $WO_2(acac)_2$  precursor, are more stable during treatment with aqueous  $H_2O_2$  than material **A**, obtained through one-pot modification of tungsten ethoxide with acetylacetonate. According to the elemental analysis data, tungsten leaching was less under the following conditions: (i) when treated with  $H_2O_2$  rather than with boiling water and (ii) when initial W content was minimal, i.e., for **B-1** and **A-1** samples in contrast to **B-1.4** and **A-2**, respectively (Table S1).

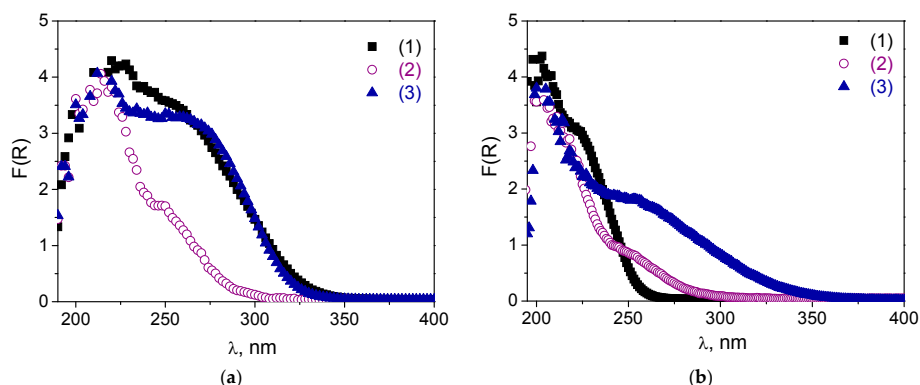


**Figure 5.** DR UV-vis spectra of calcined (a) B-1 and (b) C-1: (1) initial; (2) after treatment with boiled water for 6 h, and (3) after treatment with aqueous H<sub>2</sub>O<sub>2</sub> in CH<sub>3</sub>CN (25 °C, 1 h).

### 2.3. Catalytic Studies

The catalytic properties of the tungsten-based silicates prepared by the EISA methodology was examined during the oxidation of cyclooctene (CyOct) as a model substrate with 1 equivalent of hydrogen peroxide using CH<sub>3</sub>CN as the solvent. The main results are presented in Table 2.

**Table 2.** Oxidation of CyOct with H<sub>2</sub>O<sub>2</sub>.

Entry	Catalyst	Oxidant	Time, h	Substrate Conversion, %	TOF <sup>a</sup> , h <sup>-1</sup>	CyOct Oxide Selectivity, %	W Leaching, ppm
1	-	30% H <sub>2</sub> O <sub>2</sub>	1.5	3	-	17	-
2	A-2	30% H <sub>2</sub> O <sub>2</sub>	2	74	53	>99	55
3		50% H <sub>2</sub> O <sub>2</sub>	2	61	54	>99	36
4	A-1	30% H <sub>2</sub> O <sub>2</sub>	2	66	53	98 <sup>b</sup>	55
5		50% H <sub>2</sub> O <sub>2</sub>	2	56	54	98 <sup>b</sup>	24
6	B-1.4	30% H <sub>2</sub> O <sub>2</sub>	2	65	63	94 <sup>b</sup>	50
7		50% H <sub>2</sub> O <sub>2</sub>	2	60	65	93 <sup>b</sup>	52
8	B-1	30% H <sub>2</sub> O <sub>2</sub>	2	62	58	98 <sup>b</sup>	45
9		50% H <sub>2</sub> O <sub>2</sub>	2	57	65	>99	17
10	C-1	30% H <sub>2</sub> O <sub>2</sub>	2	68	66	97 <sup>b</sup>	58
11		50% H <sub>2</sub> O <sub>2</sub>	2	66	64	96 <sup>b</sup>	20
12	WO <sub>2</sub> (acac) <sub>2</sub>	30% H <sub>2</sub> O <sub>2</sub>	2	85	95	99 <sup>b</sup>	-
13	WO <sub>3</sub>	30% H <sub>2</sub> O <sub>2</sub>	2.5	14	13	43	-
14	SiO <sub>2</sub> -EISA <sup>c</sup>	30% H <sub>2</sub> O <sub>2</sub>	2	12	-	8	-

Reaction conditions: CyOct 0.1 mmol, H<sub>2</sub>O<sub>2</sub> (30 or 50% aqueous solution) 0.1 mmol, catalyst 0.001 mmol of W, CH<sub>3</sub>CN 1 mL, 50 °C. <sup>a</sup> TOF = (moles of substrate consumed)/(moles of W × time), determined by GC from initial rates of substrate consumption; <sup>b</sup> 1,2-Cyclooctanediol was also formed; <sup>c</sup> Catalyst SiO<sub>2</sub>-EISA matrix 15 mg.

All the elaborated W-MMM-E materials exhibited excellent selectivity during CyOct epoxidation with aqueous H<sub>2</sub>O<sub>2</sub>, regardless of the synthesis procedure, the content or the state of W (isolated or oligomeric). Catalysts B and C were somewhat more active than material A (turnover frequency (TOF) values 58–66 vs. 53, Table 2). Importantly, tungsten-free silica matrix was almost inactive in this reaction, indicating that the observed catalysis is due to the presence of W (Table 2, entry 14). Bulk tungsten oxide also had very low activity (Table 2, entry 13), which is consistent with the literature [22–24,43]. It was reported previously that only nanoparticulate WO<sub>3</sub> demonstrates catalytic activity [22,43]. The acetylacetonate complex, WO<sub>2</sub>(acac)<sub>2</sub>, was more active than heterogeneous catalysts obtained using this precursor (compare entry 12 and entries 6, 8, and 10 in Table 2); however, the latter can be used repeatedly (see Section 2.4) and thus, allows higher total turnover number (TON) values to be reached (226–237 for four consecutive runs using B-1 or C-1 vs. 85 for one run with homogeneous WO<sub>2</sub>(acac)<sub>2</sub>). Among other known tungsten-silicates, a superior CyOct epoxide yield was reported for W-MCM-41 (Si/W = 31) synthesized via the peroxide

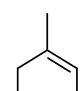
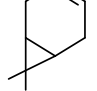
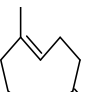
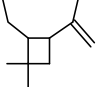
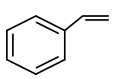
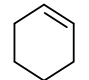
route: 100% selectivity was reached at 98% substrate conversion after 24 h at room temperature using a five-fold excess of anhydrous H<sub>2</sub>O<sub>2</sub> (solution in *t*-BuOH) [21].

As has already been mentioned, the main drawback of tungsten-containing mesoporous silicates is active metal leaching under turnover conditions during liquid-phase oxidation. Unfortunately, the amount of leached tungsten using W-MMM-E catalysts in CyOct oxidation with 30% aqueous H<sub>2</sub>O<sub>2</sub> was considerable (50–58 ppm, see Table 2). However, the leaching degree could be reduced to 17–20 ppm by using 50% hydrogen peroxide instead of 30%, or by using catalysts with a lower tungsten content (Table 2), which is in agreement with the literature [39] and our results for the catalyst's stability to aqueous H<sub>2</sub>O<sub>2</sub> and boiled water (see Section 2.2). It is quite typical of mesoporous metal-silicates that metal leaching is caused by cooperative action of H<sub>2</sub>O<sub>2</sub> and water (a combination of hydrolysis and complexing processes) [20]. Thus, it can be reduced by decreasing the water content in the reaction mixture, i.e., by using more concentrated H<sub>2</sub>O<sub>2</sub>.

Despite appreciable leaching of the active metal under turnover conditions of CyOct oxidation with 30% H<sub>2</sub>O<sub>2</sub>, hot filtration tests exhibited neither substrate conversion nor epoxide formation in the filtrate after removal of the solid catalyst (Figure 5a and Figure S3), implying that inactive metal species leached out and corroborated the heterogeneous nature of the catalysis over W-MMM-E. These results are not surprising considering that bulk WO<sub>3</sub> was almost inactive during CyOct oxidation. The same behavior was reported for the W-SBA-16 and W-KIT-6 materials [23,24]. It was suggested that the epoxidation activity is mainly due to framework-incorporated W species and not the extra-framework metal oxide species [23,24].

A range of alkenes, including bulky terpenes (3-carene and caryophyllene), can be epoxidized effectively producing epoxides with up to 99% selectivity (Table 3).

**Table 3.** Oxidation of alkenes with 50% aqueous H<sub>2</sub>O<sub>2</sub> over MMM-E catalysts.

Entry	Substrate	Catalyst	Time, h	Substrate Conversion, %	Epoxide Selectivity, %
1		A-1	5	28	82
2		C-1	5	29	85
3		A-1	3	77	99
4		C-1	3	80	>99
5		A-1 <sup>a</sup>	3	23	45 <sup>b</sup>
6		C-1 <sup>a</sup>	3	22	53 <sup>c</sup>
7		Nb-MMM-E <sup>d</sup>	3	26	39 <sup>e</sup>
8		Ti-MMM-E <sup>d</sup>	4	33	46 <sup>f</sup>
9		A-1 <sup>a</sup>	1.5	32	81 <sup>g</sup>
10		C-1 <sup>a</sup>	1	30	83 <sup>h</sup>
11		Nb-MMM-E <sup>d</sup>	0.5	30	70 <sup>i</sup>
12		Ti-MMM-E <sup>d</sup>	2.5	35	65 <sup>i</sup>

Reaction conditions: substrate 0.1 mmol, H<sub>2</sub>O<sub>2</sub> (50% aqueous solution) 0.1 mmol, catalyst 0.001 mmol W, CH<sub>3</sub>CN 1 mL, 50 °C. <sup>a</sup> 0.003 mmol W; <sup>b</sup> Other products: benzaldehyde (39%), benzoic acid (8%), and 1-phenyl-1,2-ethanediol (6%); <sup>c</sup> Other products: benzaldehyde (41%), benzoic acid (2%), and 1-phenyl-1,2-ethanediol (3%); <sup>d</sup> Catalyst 0.003 mmol Nb or Ti; <sup>e</sup> Other products: benzaldehyde (46%), benzoic acid (4%), and 1-phenyl-1,2-ethanediol (8%); <sup>f</sup> Other products: benzaldehyde (43%) and 1-phenyl-1,2-ethanediol (7%); <sup>g</sup> Heterolytic pathway selectivity = Σ(cyclohexene oxide (28%) + 2-hydroxy-cyclohexane-1-one (19%) + 1,2-trans-cyclohexane diol (34%)). Other products: 2-cyclohexene-1-ol (6%), 2-cyclohexene-1-one (6%), cyclohexenyl hydroperoxide (3%); <sup>h</sup> Heterolytic pathway selectivity = Σ(cyclohexene oxide (33%) + 2-hydroxy-cyclohexane-1-one (17%) + 1,2-trans-cyclohexane diol (33%)). Other products: 2-cyclohexene-1-ol (7%), 2-cyclohexene-1-one (7%), cyclohexenyl hydroperoxide (3%); <sup>i</sup> Total selectivity of heterolytic oxidation products (cyclohexene oxide + trans-cyclohexane-1,2-diol + 2-hydroxycyclohexanone) [59].



Styrene and cyclohexene, the substrates which are difficult to epoxidize, showed moderate epoxide selectivity (Table 3, entries 5, 6 and 9, 10). During styrene oxidation, the main byproduct was benzaldehyde (39–41%). Note that the oxidative C=C cleavage producing benzaldehyde is a typical side reaction for styrene epoxidation, specifically with H<sub>2</sub>O<sub>2</sub>, in the presence of W-based catalysts [60,61]. Cyclohexene also produced allylic oxidation products—cyclohexenyl hydroperoxide, 2-cyclohexene-1-ol, and 2-cyclohexene-1-one (totally 15–17%)—as well as 1,2-trans-cyclohexane diol and its overoxidation product, 2-hydroxycyclohexane-1-one. However, compared to Ti- and Nb-containing MMM-E (Table 3, entries 7, 8 and 11, 12), W-MMM-E materials were more selective during epoxidation of cyclohexene and styrene [59]. As with the other known tungsten–silicates, W-HMS gave only 2-cyclohexenol and 2-cyclohexenone during cyclohexene oxidation with a three-fold excess of 37% H<sub>2</sub>O<sub>2</sub> [38], while the reaction over W-SBA-16 yielded a 56% epoxidation selectivity with 36% conversion (1 equivalent of 30% H<sub>2</sub>O<sub>2</sub>, 50 °C, 6 h) [23].

We also tested the catalytic activity of the elaborated W-MMM-E materials during the oxidation of methyl phenyl sulfide (MPS) to methyl phenyl sulfoxide (MPSO) at room temperature. The results are presented in Table 4. All the samples demonstrated a similar catalytic performance during the reaction: 82–89% selectivity to MPSO at 95–98% MPS conversion. **C-1** was a bit more selective to the sulfoxide (89%), but, at the same time, the oxidant utilization efficiency in its presence was smaller in comparison to another catalyst: 89% vs. 97% for **B-1.4** and **B-1**. It is noteworthy that methyl phenyl sulfone (MPSO<sub>2</sub>) was also formed as the concomitant product. As in the case of CyOct epoxidation, tungsten-free silica matrix was almost inactive (Table 4, entry 6). Homogeneous WO<sub>2</sub>(acac)<sub>2</sub> was as active as heterogeneous ones but gave more sulfone product (compare entry 5 and entries 2–4 in Table 4).

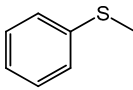
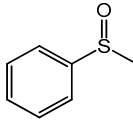
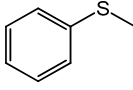
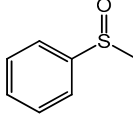
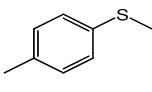
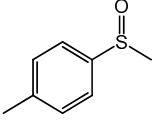
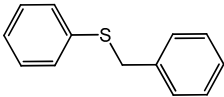
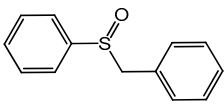
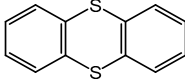
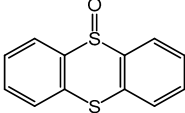
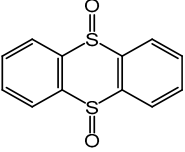
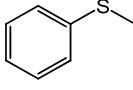
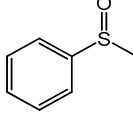
**Table 4.** Oxidation of methyl phenyl sulfide (MPS) with 30% aqueous H<sub>2</sub>O<sub>2</sub> over W-MMM-E.

Entry	Catalyst	MPS Conversion, %	MPSO Yield <sup>a</sup> , %	MPSO <sub>2</sub> Yield <sup>a</sup> , %	H <sub>2</sub> O <sub>2</sub> Efficiency, %
1	<b>A-1</b>	95	81 (85)	14 (15)	91
2	<b>B-1.4</b>	99	80 (82)	19 (18)	98
3	<b>B-1</b>	98	80 (82)	18 (18)	97
4	<b>C-1</b>	96	85 (89)	11 (11)	89
5	WO <sub>2</sub> (acac) <sub>2</sub>	100	79 (79)	21 (21)	100
6	SiO <sub>2</sub> -EISA <sup>b</sup>	7	7 (100)	0 (0)	-

Reaction conditions: MPS 0.1 mmol, H<sub>2</sub>O<sub>2</sub> (30% aqueous solution) 0.12 mmol, catalyst 0.001 mmol W, CH<sub>3</sub>CN 1 mL, 25 °C, 5 h. <sup>a</sup> Selectivity is given in parentheses; <sup>b</sup> Catalyst SiO<sub>2</sub>-EISA matrix 23 mg.

All further studies were performed in the presence of **C-1**. The decrease in the H<sub>2</sub>O<sub>2</sub>/MPS molar ratio, from 1.2 to 1 mol/mol, led to a decrease in substrate conversion, from 96 to 91%, but did not affect the selectivity of MPSO (Table 5, entries 1 and 2). The efficiency of oxidant utilization also improved from 89 to 99%. Importantly, tungsten leaching in these reactions did not exceed 3 ppm.

**Table 5.** Oxidation of various sulfides with H<sub>2</sub>O<sub>2</sub> and *tert*-butylhydroperoxide (TBHP) over C-1.

Entry	Sulfide	Conversion, %	Sulfoxide	Selectivity <sup>a</sup> , %	H <sub>2</sub> O <sub>2</sub> efficiency, %
1		91		91	99
2 <sup>b</sup>		96		89	89
3		84		88	94
4		85		84	97
5 <sup>c</sup>		68		59	100
				35	
6 <sup>d</sup>		86		95	90

Reaction conditions: sulfide 0.1 mmol, H<sub>2</sub>O<sub>2</sub> (30% aqueous solution) 0.1 mmol, catalyst 0.001 mmol W, CH<sub>3</sub>CN 1 mL, 25 °C, 4 h<sup>a</sup> Sulfone is the second product; <sup>b</sup> Sulfide 0.1 mmol, H<sub>2</sub>O<sub>2</sub> 30% aqueous solution 0.12 mmol, catalyst 0.001 mmol W, CH<sub>3</sub>CN 1 mL, 25 °C, 4 h; <sup>c</sup> Thianthrene 0.025 mmol, H<sub>2</sub>O<sub>2</sub>, 30% aqueous solution 0.025 mmol, catalyst 0.0005 mmol W, CH<sub>3</sub>CN 1 mL, 25 °C, 24 h; <sup>d</sup> Methyl phenyl sulfide 0.2 mmol, TBHP 70% aqueous solution 0.2 mmol, catalyst 0.002 mmol W, CH<sub>3</sub>CN 1 mL, 60 °C, 7 h.

Table 6 shows a comparison of the catalytic performance of W-MMM-E in MPS sulfoxidation with Ti- and Nb-MMM-E prepared by the same methodology [47,48]. One can see that tungsten-silicate C-1 demonstrated superior catalytic properties in terms of activity (TOF 120 vs. 45 and 90 h<sup>-1</sup> for Ti- and Nb-MMM-E, respectively), total MPS conversion (91% vs. 82–83%), and sulfoxidation selectivity (91% vs. 81–82%) at similar values of H<sub>2</sub>O<sub>2</sub> utilization efficiency (99% vs. 97–99%).

**Table 6.** Oxidation of MPS with 30% aqueous H<sub>2</sub>O<sub>2</sub> over different M-MMM-E.

Entry	Catalyst	MPS Conversion, %	MPSO Yield <sup>a</sup> , %	MPSO <sub>2</sub> Yield <sup>a</sup> , %	H <sub>2</sub> O <sub>2</sub> Efficiency, %	TOF, h <sup>-1</sup>
1	C-1	91	83 (91)	8 (9)	99	120
2	Ti-MMM-E	82	67 (82)	15 (18)	97	45
3	Nb-MMM-E	83	67 (81)	16 (19)	99	90

Reaction conditions: MPS 0.1 mmol, H<sub>2</sub>O<sub>2</sub> (30% aqueous solution) 0.1 mmol, catalyst 0.001 mmol W, Ti or Nb, CH<sub>3</sub>CN 1 mL, 25 °C, 5 h. <sup>a</sup> Selectivity is given in parentheses.

To evaluate the substrate scope, we studied the catalytic performance of C-1 during the oxidation of a range of organic sulfides (Table 5, entries 3–5). The results of the oxidation of methyl p-tolyl sulfide and benzyl phenyl sulfide were close to those for MPS oxidation: the sulfide conversions attained were 84% and 85% and the selectivities to corresponding sulfoxides were 88 and 84%, respectively. During thianthrene oxidation, products of electrophilic oxidation, namely thianthrene-5-oxide and thianthrene-5,10-dioxide, were mainly formed (Table 5, entry 5).

C-1 also catalyzed the oxidation of MPS with another oxidant, *tert*-butylhydroperoxide (TBHP) (Table 5, entry 6). In this case, the reaction was more selective to sulfoxide: selectivity reached 95% at 86% substrate conversion, but required a higher reaction temperature, 60 °C.

#### 2.4. Catalyst Recyclability and Stability under Reaction Conditions

The hot catalyst filtration test for MPS oxidation indicated the heterogeneous nature of the catalysis over W-MMM-E (Figure 6b), which was anticipated given that the tungsten leaching was negligible (2.5–3 ppm) under the turnover conditions of MPS oxidation, i.e., at room temperature instead of the 50 °C used for CyOct oxidation.

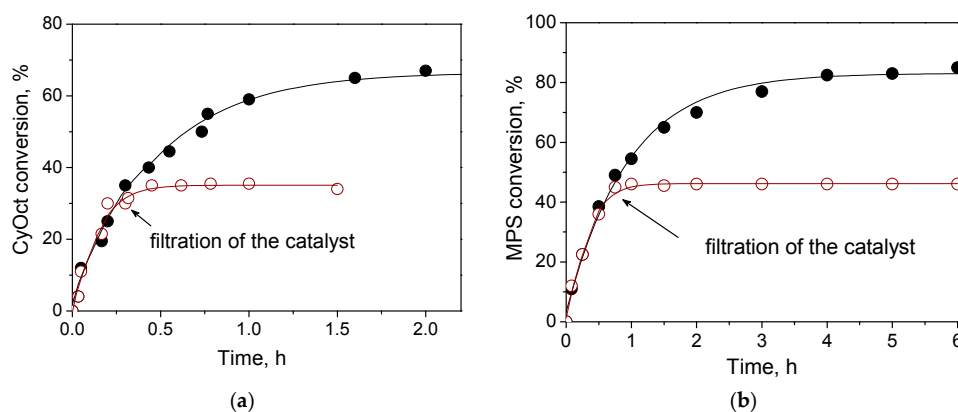


**Figure 6.** Hot catalyst filtration test for (a) CyOct oxidation with 30% H<sub>2</sub>O<sub>2</sub> over C-1 and (b) MPS oxidation with 30% H<sub>2</sub>O<sub>2</sub> over B-1. Reaction conditions: (a) CyOct 0.1 mmol, H<sub>2</sub>O<sub>2</sub> 0.1 mmol, catalyst 0.001 mmol W, CH<sub>3</sub>CN 1 mL, 50 °C; (b) MPS 0.1 mmol, H<sub>2</sub>O<sub>2</sub> 0.1 mmol, W-EISA 0.001 mmol W, CH<sub>3</sub>CN 1 mL, 25 °C. (●) CyOct or MPS conversion in the presence of catalyst and (○) experiment with hot catalyst filtration.

Although the question on the catalyst stability under turnover conditions is crucial for heterogeneous catalysis during liquid-phase processes [62], only a few examples on the reusability of tungsten-based mesoporous silicates in the oxidations with aqueous H<sub>2</sub>O<sub>2</sub> have been so far reported [22,23,32,37,39]. Good recyclability within 3–5 consecutive runs was shown for (i) W-MCM-48 with a 38.5 Si/W molar ratio during cyclopentene oxidation with a two-fold excess of 50% H<sub>2</sub>O<sub>2</sub> (35 °C, 35 h) [32]; (ii) WO<sub>3</sub>-MCF washed with ammonium acetate (Si/W = 941.7) during cycloocta-1,5-diene epoxidation with a three-fold excess of 50% H<sub>2</sub>O<sub>2</sub> (60 °C, 24 h) [39]; and (iii) nanoparticulate WO<sub>3</sub> prepared by flame spray pyrolysis during oxidation of cyclooctene with 1 equiv. H<sub>2</sub>O<sub>2</sub> (80 °C, 4 h) [22].

W-HMS (Si/W = 30) [37] and W-SBA-16 (Si/W = 22) [23] demonstrated deterioration of catalytic properties upon reuse.

The recycling behavior of all the elaborated W-MMM-E catalysts was studied in three to four consecutive runs of the oxidation of CyOct with 30 or 50% H<sub>2</sub>O<sub>2</sub> (Figures S5–S7 and Figure 7a–c). In contrast to Nb-MMM-E catalysts, calcination was necessary to regenerate the catalyst (Figure S7 and Figure 7b). In good agreement with the leaching tests, better recycling behavior was observed when using 50% H<sub>2</sub>O<sub>2</sub> instead of 30%. One can see that A catalysts exhibited a gradual decrease in the maximal achievable substrate conversion during recycling at stably high epoxidation selectivity levels when using 30% aqueous H<sub>2</sub>O<sub>2</sub> (Figures S5a and S6). The A-2 catalyst showed stability of catalytic properties after the first reuse with 50% H<sub>2</sub>O<sub>2</sub> as the oxidant and then activity smoothly reduced (CyOct conversion decreased from 61% to 55% after the second reuse; Figure S4b), while A-1 lost neither activity nor selectivity during recycling using 50% H<sub>2</sub>O<sub>2</sub> (Figure 7a). The B-1.4 sample turned out to be slightly less stable than A-2: the value of CyOct conversion reduced from 61% to 42% after the second reuse using 50% H<sub>2</sub>O<sub>2</sub> (Figure S7). Both B-1 and C-1 catalysts showed good recycling behavior using 50% H<sub>2</sub>O<sub>2</sub> (Figure 7b,c). Thus, one may conclude that there is no necessity for eliminating water content in the reaction mixture during W-MMM-E synthesis or using isolated WO<sub>2</sub>(acac)<sub>2</sub> as the tungsten precursor, since all A-1, B-1 and C-1 samples showed good stability of catalytic properties during reuse (compare Figure 7a–c). Under the milder conditions of MPS oxidation (25 °C), catalyst C-1 did not lose its catalytic properties during at least five consecutive reuses using 30% aqueous H<sub>2</sub>O<sub>2</sub> (Figure 7d). Tungsten leaching was 17–24 and 2.5 ppm after the first run of CyOct (see Table 2) and MPS oxidation, respectively, over the fresh catalysts. With the reused C-1 catalyst, the degree of W leaching reduced to 7.5 (for CyOct) and <1 ppm (for MPS).

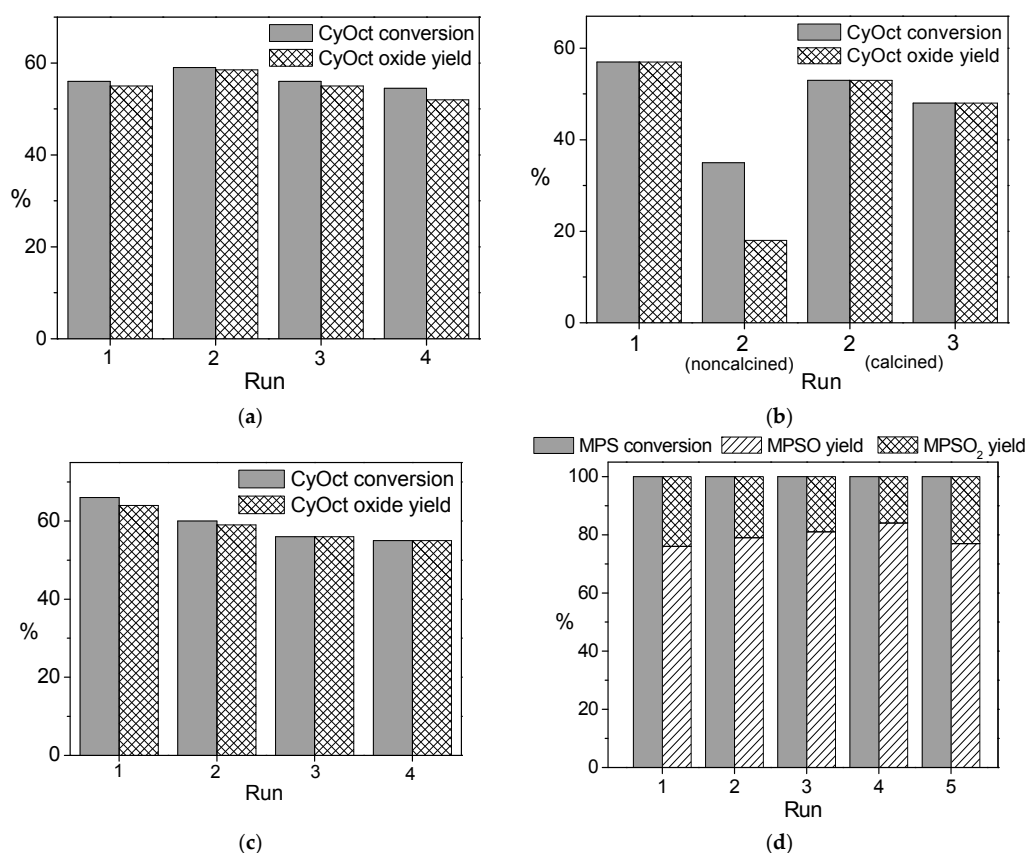


**Figure 7.** Reuse of (a) A-1; (b) B-1; and (c) C-1 during CyOct oxidation with 50% H<sub>2</sub>O<sub>2</sub>; and (d) C-1 during MPS oxidation with 30% H<sub>2</sub>O<sub>2</sub>. Reaction conditions: (a–c) CyOct 0.1 M, H<sub>2</sub>O<sub>2</sub> 0.1 M, catalyst 60 mg, CH<sub>3</sub>CN 2 mL, 50 °C, 3 h; (d) MPS 0.1 M, H<sub>2</sub>O<sub>2</sub> 0.12 M, catalyst 70 mg, CH<sub>3</sub>CN 3 mL, 25 °C, 4 h.

Raman spectra of catalysts **A-1** and **A-2** revealed no changes concerning the band attributed to  $\nu(W=O)$  at  $975\text{ cm}^{-1}$  after CyOct catalytic oxidation Figure 3, curves (7) and (8)). However, the low-intensity band at ca.  $600\text{ cm}^{-1}$ , that refers to the spectrum of the tungsten-free silicate matrix decreased. Supposedly, this may be caused by some restructuring of the silica wall in the mesoporous material as a result of wetting and repeated calcinations after catalytic reactions. However, this does not affect the long-range ordering of the mesoporous material, since the textural properties of the **A-1** sample changed insignificantly after the catalytic reaction of CyOct oxidation (see Table 1). The observed long-wave shift in the DR UV-vis spectra (Figure 8a,b) of non-calcined catalysts **A-1** and **A-2** after the oxidation reaction may be due to adsorption of water or some organic molecules. Indeed, the DR UV-vis spectra after subsequent calcination revealed almost no changes compared to the spectrum of initial materials, **A-1** and **A-2** (Figure 8a,b).

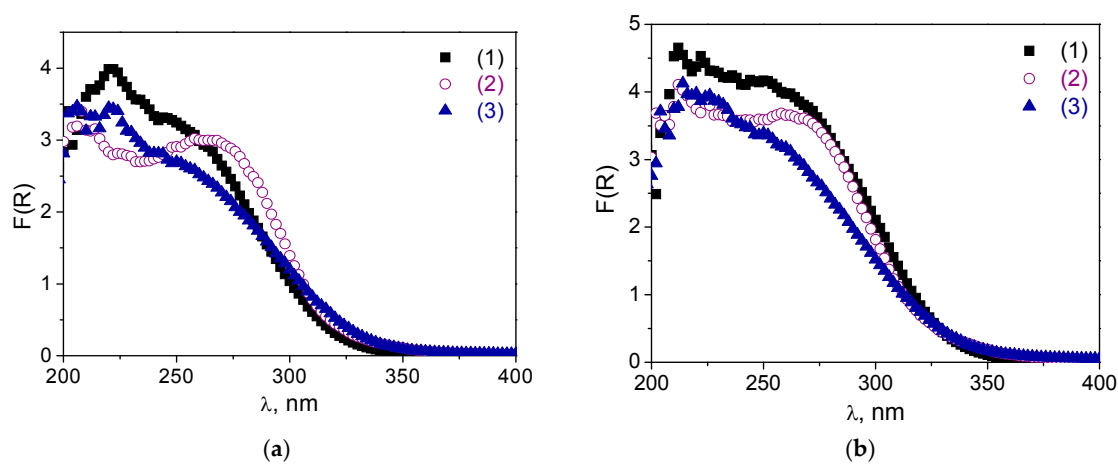


**Figure 8.** DR UV-vis spectra of (a) **A-1** and (b) **A-2**: (1) initial calcined; (2) and (3) after catalytic reaction of CyOct oxidation—uncalcined and calcined, respectively. Reaction conditions: CyOct 0.1 mmol,  $H_2O_2$  0.1 mmol, catalyst 0.001 mmol W,  $CH_3CN$  1 mL,  $50\text{ }^\circ\text{C}$ .

### 3. Materials and Methods

#### 3.1. Materials

CTAB (>99%), TEOS (>98%), and tungsten(VI) dichloride dioxide  $WO_2Cl_2$  (99%) were purchased from Aldrich. Tungsten(VI) ethoxide was used as received from Alfa Aesar (Ward Hill, MA, USA). Acetonitrile (HPLC-grade, Panreac Chimica S.A.U., Barcelona, Spain) was dried and stored over activated  $4\text{ \AA}$  molecular sieves. Ethanol (95%), ethylacetate and other reactants were obtained commercially and used without any additional purification. The concentration of  $H_2O_2$  (30 or 50 wt % in water) was determined iodometrically prior to use. Deionized water (EASY pure, RF, Barnsted) was used for the preparation of catalysts.

#### 3.2. Catalyst Preparation and Characterization

##### 3.2.1. Method A

*Synthesis of tungsten precursor.* A typical procedure was as follows: dry ethylacetate (3.0 mL) was mixed with acetylacetone (acac, 0.08 mL, 0.8 mmol) and then tungsten(VI) ethoxide (0.08 g, 0.18 mmol) was added. The reaction mixture was stirred at  $80\text{ }^\circ\text{C}$  for one hour. Subsequently, the formed solution of tungsten acetylacetonate complex was filtered to remove any insoluble impurities and was used for the synthesis of tungsten silicates.

*Synthesis of W,Si-catalysts.* In a standard procedure, the surfactant, CTAB (2.75 g, 7.5 mmol) was dissolved in ethanol (95%, 73 mL) under vigorous stirring for 2 h at room temperature. Then, TEOS



(11.2 mL, 0.05 mol), deionized H<sub>2</sub>O (6 mL), 36% HCl (6 µL, 0.07 mmol) and the solution of the tungsten precursor (see above) were added under vigorous stirring. The reaction mixture was stirred (750 rpm) for 30 s and then the resulting clear solution was left in an open Petri dish under ambient conditions until full evaporation of the solvent. The as-made solid was calcined at 550 °C for 5 h in air with a temperature ramp of 1 °C/min to remove the organic species. The tungsten content, calculated based on the Si/W molar ratio used in the synthesis, was 1.0 wt %; thus, the solid was designated as **A-1**.

For the preparation of the **A-2** sample, the reagent loadings during the synthesis of the tungsten precursor were increased twice (ethylacetate 6.0 mL, acetylacetone 0.15 mL, 1.5 mmol, tungsten(VI) ethoxide 0.16 g, 0.35 mmol), with reagent loadings used in the step of preparation of tungsten silicate remaining the same. CTAB (2.75 g, 7.5 mmol) was dissolved in 73 mL of 95% ethanol under vigorous stirring (2 h, room temperature) followed by addition of TEOS (11.2 mL, 0.05 mol), deionized H<sub>2</sub>O (6 mL), 36% HCl (6 µL, 0.07 mmol) and solution of tungsten precursor. The remaining steps were the same as in the synthesis of **A-1**. The tungsten content, calculated based on Si/W molar ratio used in the synthesis, was 2.0 wt %; thus, the solid was designated as **A-2**.

### 3.2.2. Method B

*Synthesis of the tungsten precursor, WO<sub>2</sub>(acac)<sub>2</sub>.* WO<sub>2</sub>(acac)<sub>2</sub> was prepared following a slight modification of the procedure reported in [63]. WO<sub>2</sub>Cl<sub>2</sub> (0.61 g, 2.2 mmol) and excess acac (4 mL, 0.039 mol) were added to dried toluene (10 mL), and then the resulting solution was refluxed for 20 h. After that, the hot reaction mixture was filtered. After removal of volatiles under vacuum, the solid residue was recrystallized twice from dry diethyl ether to give a yield of: 0.61 g (70%). The structure of WO<sub>2</sub>(acac)<sub>2</sub> was confirmed by UV-Vis and <sup>1</sup>H NMR spectroscopy [63–65].

*Synthesis of W,Si-catalysts.* CTAB (2.75 g, 7.5 mmol) was dissolved in 73 mL of dry ethanol under vigorous stirring for 2 h at room temperature. Then, TEOS (11.2 mL, 0.05 mol) and the solution of the WO<sub>2</sub>(acac)<sub>2</sub> precursor (0.1 g, 0.24 mmol) in 3 mL of dry acac were added under vigorous stirring. The reaction mixture was stirred (750 rpm) for 30 s and then put into a Petri dish and left under ambient conditions until full evaporation of the solvent. The as-made solid was calcined at 550 °C for 5 h in air with a temperature ramp of 1 °C/min to remove the organic species. The tungsten content, according to the Si/W molar ratio used in the synthesis, was 1.4 wt %, and the solid was designated as **B-1.4**. For the synthesis of the **B-1** sample, the amount of WO<sub>2</sub>(acac)<sub>2</sub> precursor was decreased to 0.07 g (0.017 mmol) with other loadings remaining the same.

### 3.2.3. Method C

The synthesis procedure was similar to the protocol described for **B-1**, but 95% ethanol was used (73 mL) and 36% HCl (6 µL) was added along with deionized water (6 mL). CTAB (2.75 g, 7.5 mmol) was dissolved in ethanol (95%, 73 mL) under vigorous stirring (2 h, room temperature). Then, TEOS (11.2 mL, 0.05 mol), deionized H<sub>2</sub>O (6 mL), 36% HCl (6 µL, 0.07 mmol) and solution of the WO<sub>2</sub>(acac)<sub>2</sub> precursor (0.07 g, 0.017 mmol) in 3 mL of dry acac were added under vigorous stirring. The reaction mixture was stirred (750 rpm) for 30 s and then put into a Petri dish and left under ambient conditions until full evaporation of the solvent. The as-made solid was calcined at 550 °C for 5 h in air (1 °C/min) to remove the organic species. The tungsten content, according to the Si/W molar ratio used in the synthesis, was 1.0 wt %, and the solid was designated as **C-1**.

### 3.2.4. Preparation of Silica Matrix

A W-free silica matrix, SiO<sub>2</sub>-EISA, was prepared following a similar procedure but without adding any W-precursor or acac: 2.75 g of CTAB was dissolved in 57 g of ethanol (95%) for 2 h at room temperature. Then, 10.4 g of TEOS and 6.0 g of 0.01 M HCl were added under vigorous stirring. The resulting clear solution was left in an open Petri dish under ambient conditions until full evaporation of the solvent. The as-made solid was calcined at 550 °C for 5 h in air.

All freshly calcined samples (if not stated otherwise) were characterized by elemental analysis, N<sub>2</sub> adsorption, X-ray diffraction (XRD), Raman and diffusion reflectance UV-vis (DR UV-vis) spectroscopic techniques.

### 3.3. Hydrothermal Stability and Stability towards Aqueous H<sub>2</sub>O<sub>2</sub>

To estimate the stability of the samples, they were treated either with boiled water for 6 h (150 mg catalyst, 15 mL H<sub>2</sub>O) or with aqueous 30% H<sub>2</sub>O<sub>2</sub> for 1 h (100 mg of catalyst, 0.11 M H<sub>2</sub>O<sub>2</sub>, 20 mL CH<sub>3</sub>CN, 25 °C), dried in air and calcined at 550 °C before physicochemical measurements.

### 3.4. Catalytic Oxidations

Catalytic oxidations were performed under vigorous stirring (500 rpm) in thermostated glass vessels. Typical reaction conditions for alkene epoxidation were as follows: alkene 0.1 mmol, H<sub>2</sub>O<sub>2</sub> 0.1 mmol, catalyst 0.001 mmol W, CH<sub>3</sub>CN 1 mL, 50 °C. Sulfoxidation reactions were performed under the following reaction conditions: sulfide 0.1–0.2 mmol, H<sub>2</sub>O<sub>2</sub> 0.1–0.12 mmol or TBHP 0.2 mmol, catalyst 0.001–0.002 mmol W, CH<sub>3</sub>CN 1 mL, 25–60 °C. Thianthrene oxidation was carried out using 0.025 M substrate and H<sub>2</sub>O<sub>2</sub>, 0.5 μmol of W (C-1 catalyst) in 1 mL of CH<sub>3</sub>CN at 25 °C for 24 h. Reactions were started by the addition of an oxidant. Samples of the reaction mixture (0.1 μL) were withdrawn periodically during the reaction course by a syringe. The oxidation products were identified by gas chromatography–mass spectrometry (GC–MS) and <sup>1</sup>H NMR using authentic samples. The product yields and substrate conversions were quantified by gas chromatography (GC) using an internal standard, biphenyl. MPS consumption was determined by HPLC, using biphenyl as an internal standard (ZORBAX Eclipse Plus C-18 4.6 × 150 mm, 5-Micron, H<sub>2</sub>O-*i*PrOH = 40:60, 1 mL/min, 25 °C). Aliquots of 10 μL of the reaction mixture were taken periodically by a syringe and added in *i*PrOH (100 μL) for analysis. In the oxidation of thianthrene, the substrate conversion and product yields were determined by <sup>1</sup>H NMR by integration of corresponding signals. Turnover frequency (TOF) values were determined from the initial rates of substrate consumption. Each experiment was reproduced at least two times.

Catalyst reusability was examined in 2–3 time-scaled experiments (the total reaction mixture volume 2–3 mL). After the reactions, catalysts were filtered off and washed with hot acetonitrile and acetone. Before use in the next catalytic run, the catalyst was calcined in air (if not stated otherwise) at 250 °C for 2 h and then at 550 °C for 4 h. The nature of catalysis was verified by hot catalyst filtration tests.

### 3.5. Instrumentation

GC analyses were performed using a gas chromatograph Tsvet-500 or Chromos GH-1000, equipped with a flame ionization detector and a quartz capillary column (30 m × 0.25 mm) filled with DB-5 MS (Agilent Technologies, Santa Clara, CA, USA). GC–MS analyses were carried out using an Agilent 7000B system with a triple-quadrupole mass-selective detector Agilent 7000 and a GC Agilent 7890B apparatus (quartz capillary column 30 m × 0.25 mm/HP-5 ms). HPLC analyses were performed using HPLC Agilent Technologies 1220 Infinity LC. <sup>1</sup>H NMR spectra were recorded on a Brüker AVANCE-400 spectrometer at 400.13 MHz.

XRD measurements were performed on a high precision X-ray diffractometer, mounted on beamline No. 2 of the VEPP-3 storage ring at Siberian Synchrotron Radiation Center (Novosibirsk, Russia). The radiation wavelength was 0.15393 nm. A high natural collimation of the synchrotron radiation beam, a flat perfect crystal analyzer, and a parallel Soller slit on the diffracted beam, limiting its azimuthal divergence, provided extremely high instrumental resolution in a small angle region of 2θ = 0.5–10° and higher.

Electron microscopy was performed using a JEM-2200FS (JEOL Ltd., Tokyo, Japan) electron microscope operated at 200 kV. Images with a high atomic number contrast (Z-contrast) were acquired

using a high angle annular dark field (HAADF) detector in Scanning-TEM (STEM) mode. The samples for the TEM study were prepared on perforated carbon film mounted on a copper grid.

Nitrogen adsorption measurements were carried out at 77 K using a NOVA 1200 instrument (Quantachrome Instruments, Boynton Beach, FL, USA) within the partial pressure range,  $10^{-4}$ –1.0. The catalysts were degassed at 150 °C for 24 h before the measurements. Surface areas of the W-MMM-E samples were determined by the BET analysis of low-temperature N<sub>2</sub> adsorption data. Pore size distributions were calculated from the adsorption branches of the nitrogen isotherms by means of the regularization procedure, using reference local isotherms calculated in a cylindrical silica pore model in the framework of the density functional theory (DFT) approach. Special software provided by Quantachrome Corp. was used for this purpose (NovaWin 10.01, Quantachrome Instruments, Boynton Beach, FL, USA). Mean pore diameters were calculated as mathematical expectation values from these distributions.

Tungsten content in the solids and in the filtrate, which remained after separation of the catalysts from the reaction mixture, was determined by ICP-OES using an Optima-430 DV instrument (PerkinElmer Inc., Waltham, MA, USA).

The state of tungsten in the catalysts was probed by DR UV-vis spectroscopy under ambient conditions using an UV-VIS 2501PC spectrophotometer (Shimadzu Corp., Kyoto, Japan). FT-Raman spectra (3600–100 cm<sup>-1</sup>, 300 scans, resolution 4 cm<sup>-1</sup>, 180° geometry) were recorded using a RFS 100/S spectrometer (Bruker, Billerica, MA, USA). Excitation of the 1064 nm line was provided by a Nd-YAG laser (100 mW power output).

#### 4. Conclusions

A series of mesoporous tungsten-silicates, W-MMM-E, were prepared using evaporation-induced self-assembly methodology. Two different procedures were developed: the first one involved one-pot modification of tungsten(VI) ethoxide with acetylacetone followed by the addition of silica precursor and templating agent, while the second one was based on the use of tungsten acetylacetonate, WO<sub>2</sub>(acac)<sub>2</sub>, complex as the metal source. According to DR UV-vis spectroscopy, the elaborated W-MMM-E materials contained two types of tungsten oxo species—isolated tetrahedrally coordinated and oligomeric octahedrally coordinated—with the ratio depending on the tungsten content in the catalyst. Materials with lower W contents showed a higher contribution of isolated species, regardless of the preparation method.

W-MMM-E materials produced active and highly selective catalysts for a range of epoxidation and sulfoxidation reactions using aqueous H<sub>2</sub>O<sub>2</sub>. Selectivity to epoxides, including bulky 3-carene and caryophyllene oxides, reached 85–99% at up to 80% conversion (50% H<sub>2</sub>O<sub>2</sub>, 50 °C), while sulfoxides formed with 84–90% selectivity in almost complete conversions and with a 100% H<sub>2</sub>O<sub>2</sub> utilization efficiency (30% H<sub>2</sub>O<sub>2</sub>, 25 °C). Hot filtration tests confirmed the truly heterogeneous nature of the catalysis. Compared to Ti- and Nb-MMM-E silicates synthesized using the same evaporation-induced self-assembly methodology, W-MMM-E materials were more selective in both epoxidation of alkenes and sulfoxidation of thioethers.

The stability of W-MMM-E materials to metal leaching was only slightly affected by the preparation procedure used for their synthesis, but it depended on the initial amount of tungsten in the catalyst and reaction conditions employed. Thus, in cyclooctene oxidation, which occurred at 50 °C, the amount of leached W in the reaction mixture could be reduced from 50–55 ppm to 17–20 ppm by using 50% instead of 30% aqueous H<sub>2</sub>O<sub>2</sub> as the oxidant and/or employing a catalyst containing 0.8–0.9 wt % of W instead of 1.4–1.6 wt %. In the case of sulfoxidation reactions, which easily proceeded at room temperature, the degree of tungsten leaching did not exceed 2.5–3 ppm for the catalysts with 0.8–0.9 wt % of W. The W-MMM-E catalysts with the optimal tungsten loading (0.8–0.9 wt % W) can be used repeatedly without loss of catalytic, textural and structural properties during, at least, four consecutive runs.

**Supplementary Materials:** The following are available online at <http://www.mdpi.com/2073-4344/8/3/95/s1>, Table S1: Physicochemical properties of W-MMM-E catalysts after treatment with 0.11 M H<sub>2</sub>O<sub>2</sub> or boiled water, Figure S1: XRD pattern of calcined A-1 catalyst, Figure S2: DR UV-vis spectra of calcined (a) A-1 and (b) A-2: (■) initial, (●) after treatment with boiled water for 6 h, and (▲) after treatment with aqueous H<sub>2</sub>O<sub>2</sub> in CH<sub>3</sub>CN (25 °C, 1 h), Figure S3: DR UV-vis spectra of calcined B-1.4: (■) initial, (●) after treatment with boiled water for 6 h, and (▲) after treatment with aqueous H<sub>2</sub>O<sub>2</sub> in CH<sub>3</sub>CN (25 °C, 1 h), Figure S4: Hot catalyst filtration test for CyOct oxidation over (a) A-2, (b) A-1, (c) B-1.4, and (d) B-1. Reaction conditions: CyOct 0.1 mmol, H<sub>2</sub>O<sub>2</sub> (30% aqueous solution) 0.1 mmol, catalyst 0.001 mmol of W; CH<sub>3</sub>CN 1 mL, 50 °C. (○) CyOct conversion after hot catalyst filtration, Figure S5: Reuse of A-2 in CyOct oxidation with (a) 30% H<sub>2</sub>O<sub>2</sub> and (b) 50% H<sub>2</sub>O<sub>2</sub>. Reaction conditions: CyOct 0.1 M, H<sub>2</sub>O<sub>2</sub> 0.1 M, catalyst 30 mg, CH<sub>3</sub>CN 2 mL, 50 °C, Figure S6: Reuse of A-1 in CyOct oxidation with 30% H<sub>2</sub>O<sub>2</sub>. Reaction conditions: CyOct 0.1 M, H<sub>2</sub>O<sub>2</sub> 0.1 M, catalyst 60 mg, CH<sub>3</sub>CN 2 mL, 50 °C, Figure S7: Reuse of B-1.4 in CyOct oxidation with 50% H<sub>2</sub>O<sub>2</sub>. Reaction conditions: CyOct 0.1 M, H<sub>2</sub>O<sub>2</sub> 0.1 M, catalyst 40 mg, CH<sub>3</sub>CN 2 mL, 50 °C.

**Acknowledgments:** The help of Mikhail V. Shashkov, Igor Y. Skobelev, and Svetlana A. Yashnik, in GC-MS, N<sub>2</sub> adsorption, and DRS UV-vis measurements, respectively, is greatly appreciated. This work was conducted within the framework of the budget project for the Borekov Institute of Catalysis. The research activity was partially supported by the Russian Foundation for Basic Research (RFBR grant # 15-33-20225).

**Author Contributions:** Nataliya Maksimchuk and Olga Zalomaeva performed catalytic experiments. Irina Ivanchikova synthesized the catalysts. Yurii Chesalov, Alexandr Shmakov, and Vladimir Zaikovskii recorded Raman spectra, XRD patterns, and STEM-HAADF images, respectively. Nataliya Maksimchuk and Oxana Kholdeeva managed all the experimental and writing process as the corresponding authors.

**Conflicts of Interest:** The authors declare no conflict of interest.

## References

1. Lassner, E.; Schubert, W.-D.; Lüderitz, E.; Wolf, H.U. Tungsten, Tungsten alloys, and tungsten compounds. In *Ullmann's Encyclopedia of Industrial Chemistry*; Wiley-VCH Verlag GmbH & Co. KGaA: Weinheim, Germany, 2000.
2. Sienel, G.; Rieth, R.; Rowbottom, K.T. Epoxides. In *Ullmann's Encyclopedia of Industrial Chemistry*; Wiley-VCH Verlag GmbH & Co. KGaA: Weinheim, Germany, 2000.
3. Adolfsson, H. Transition metal-catalyzed epoxidation of alkenes. In *Modern Oxidation Methods*; Bäckvall, J.-E., Ed.; Wiley-VCH: Weinheim, Germany, 2004; pp. 21–49.
4. Venturello, C.; D'Aloisio, R.; Bart, J.C.J.; Ricci, M. A New peroxotungsten heteropoly anion with special oxidizing properties: Synthesis and structure of tetrahexylammonium tetra(diperoxotungsto)phosphate(3-). *J. Mol. Catal.* **1985**, *32*, 107–110. [[CrossRef](#)]
5. Ishii, Y.; Yamawaki, K.; Ura, T.; Yamada, H.; Yoshida, T.; Ogawa, M. Hydrogen peroxide oxidation catalyzed by heteropoly acids combined with cetylpyridinium chloride: Epoxidation of olefins and allylic alcohols, ketonization of alcohols and diols, and oxidative cleavage of 1,2-diols and olefins. *J. Org. Chem.* **1988**, *53*, 3587–3593. [[CrossRef](#)]
6. Hoegaerts, D.H.; Sels, B.F.; De Vos, D.E.; Verpoort, F.; Jacobs, P.A. Heterogeneous tungsten-based catalysts for the epoxidation of bulky olefins. *Catal. Today* **2000**, *60*, 209–218. [[CrossRef](#)]
7. Grigoropoulou, G.; Clark, J.H.; Elings, J.A. Recent developments on the epoxidation of alkenes using hydrogen peroxide as an oxidant. *Green Chem.* **2003**, *5*, 1–7. [[CrossRef](#)]
8. Brégeault, J.-M. Transition-metal complexes for liquid-phase catalytic oxidation: Some aspects of industrial reactions and of emerging technologies. *Dalton Trans.* **2003**, 3289–3302. [[CrossRef](#)]
9. Lane, B.S.; Burgess, K. Metal-catalyzed epoxidations of alkenes with hydrogen peroxide. *Chem. Rev.* **2003**, *103*, 2457–2474. [[CrossRef](#)] [[PubMed](#)]
10. Noyori, R.; Aoki, M.; Sato, K. Green oxidation with aqueous hydrogen peroxide. *Chem. Commun.* **2003**, 1977–1986. [[CrossRef](#)]
11. Kamata, K.; Yonehara, K.; Sumida, Y.; Yamaguchi, K.; Hikichi, S.; Mizuno, N. Efficient epoxidation of olefins with  $\geq 99\%$  selectivity and use of hydrogen peroxide. *Science* **2003**, *300*, 964–966. [[CrossRef](#)] [[PubMed](#)]
12. Mizuno, N.; Yamaguchi, K.; Kamata, K. Epoxidation of olefins with hydrogen peroxide catalyzed by polyoxometalates. *Coord. Chem. Rev.* **2005**, *249*, 1944–1956. [[CrossRef](#)]
13. Kim, D.S.; Ostromecki, M.; Wachs, I.E. Preparation and characterization of WO<sub>3</sub>/SiO<sub>2</sub> catalysts. *Catal. Lett.* **1995**, *33*, 209–215. [[CrossRef](#)]

14. Morey, M.; Bryan, J.; Schwarz, S.; Stucky, G. Pore Surface Functionalization of MCM-48 mesoporous silica with tungsten and molybdenum metal centers: Perspectives on catalytic peroxide activation. *Chem. Mater.* **2000**, *12*, 3435–3444. [[CrossRef](#)]
15. Rhers, B.; Salameh, A.; Baudouin, A.; Quadrelli, E.A.; Taoufik, M.; Copéret, C.; Lefebvre, F.; Basset, J.-M.; Solans-Monfort, X.; Eisenstein, O.; et al. A well-defined, silica-supported tungsten imido alkylidene olefin metathesis catalyst. *Organometallics* **2006**, *25*, 3554–3557. [[CrossRef](#)]
16. Herrera, J.E.; Kwak, J.H.; Hu, J.Z.; Wang, Y.; Peden, C.H.; Macht, J.; Iglesia, E. Synthesis, characterization, and catalytic function of novel highly dispersed tungsten oxide catalysts on mesoporous silica. *J. Catal.* **2006**, *239*, 200–211. [[CrossRef](#)]
17. Le, Y.; Yang, X.; Dai, W.-L.; Gao, R.; Fan, K. Unexpected mononuclear W(VI) complexes containing phosphonate ligands anchored on mesoporous silica. Another strategy for immobilization. *Catal. Commun.* **2008**, *9*, 1838–1841. [[CrossRef](#)]
18. Howell, J.G.; Li, Y.-P.; Bell, A.T. Propene metathesis over supported tungsten oxide catalysts: A study of active site formation. *ACS Catal.* **2016**, *6*, 7728–7738. [[CrossRef](#)]
19. *CRC Handbook of Chemistry and Physics, Internet Version 2005*; Lide, D (Ed.) CRC Press: Boca Raton, FL, USA, 2005; Available online: <http://www.hbcpnetbase.com> (accessed on 23 June 2005).
20. Kholdeeva, O.A. Selective oxidations catalyzed by mesoporous metal silicates. In *Liquid Phase Oxidation via Heterogeneous Catalysis: Organic Synthesis and Industrial Applications*; Clerici, M.G., Kholdeeva, O.A., Eds.; Wiley: Hoboken, NJ, USA, 2013; pp. 127–219.
21. Briot, E.; Piquemal, J.-Y.; Vennat, M.; Bregeault, J.-M.; Chottard, G.; Manoli, J.-M. Aqueous acidic hydrogen peroxide as an efficient medium for tungsten insertion into MCM-41 mesoporous molecular sieves with high metal dispersion. *J. Mater. Chem.* **2000**, *10*, 953–958. [[CrossRef](#)]
22. Hammond, C.; Straus, J.; Righettoni, M.; Pratsinis, S.E.; Hermans, I. Nanoparticulate tungsten oxide for catalytic epoxidations. *ACS Catal.* **2013**, *3*, 321–327. [[CrossRef](#)]
23. Maheswari, R.; Pachamuthu, M.P.; Ramanathan, A.; Subramaniam, B. Synthesis, Characterization, and epoxidation activity of tungsten-incorporated SBA-16 (W-SBA-16). *Ind. Eng. Chem. Res.* **2014**, *53*, 18833–18839. [[CrossRef](#)]
24. Yan, W.; Ramanathan, A.; Ghanta, M.; Subramaniam, B. Towards highly selective ethylene epoxidation catalysts using hydrogen peroxide and tungsten- or niobium-incorporated mesoporous silicate (KIT-6). *Catal. Sci. Technol.* **2014**, *4*, 4433–4439. [[CrossRef](#)]
25. Brégeault, J.-M.; Piquemal, J.-Y.; Briot, E.; Duprey, E.; Launay, F.; Salles, L.; Vennat, M.; Legrand, A.-P. New approaches to anchoring or inserting highly dispersed tungsten oxo(peroxo) species in mesoporous silicates. *Microporous Mesoporous Mater.* **2001**, *44–45*, 409–417. [[CrossRef](#)]
26. Zhang, Z.; Suo, J.; Zhang, X.; Li, S. Synthesis, characterization, and catalytic testing of W-MCM-41 mesoporous molecular sieves. *Appl. Catal. A Gen.* **1999**, *179*, 11–19. [[CrossRef](#)]
27. Zhang, Z.; Suo, J.; Zhang, X.; Li, S. Synthesis of highly active tungsten-containing MCM-41 mesoporous molecular, sieve catalyst. *Chem. Commun.* **1998**, *2*, 241–242. [[CrossRef](#)]
28. Dai, W.-L.; Chen, H.; Cao, Y.; Li, H.; Xie, S.; Fan, K. Novel economic and green approach to the synthesis of highly active W-MCM41 catalyst in oxidative cleavage of cyclopentene. *Chem. Commun.* **2003**, 892–893. [[CrossRef](#)]
29. Chen, H.; Dai, W.-L.; Deng, J.-F.; Fan, K. Novel Heterogeneous W-doped MCM-41 catalyst for highly selective oxidation of cyclopentene to glutaraldehyde by aqueous H<sub>2</sub>O<sub>2</sub>. *Catal. Lett.* **2002**, *81*, 131–136. [[CrossRef](#)]
30. Trens, P.; Stathopoulos, V.; Hudson, M.J.; Pomonis, P. Synthesis and characterization of packed mesoporous tungsteno-silicates: Application to the catalytic dehydrogenation of 2-propanol. *Appl. Catal. A Gen.* **2004**, *263*, 103–108. [[CrossRef](#)]
31. Klepel, O.; Bohlmann, W.; Ivanov, E.B.; Riede, V.; Papp, H. Incorporation of tungsten into MCM-41 framework. *Microporous Mesoporous Mater.* **2004**, *76*, 105–112. [[CrossRef](#)]
32. Yang, X.-L.; Dai, W.-L.; Gao, R.; Chen, H.; Li, H.; Cao, Y.; Fan, K. Synthesis, characterization and catalytic application of mesoporous W-MCM-48 for the selective oxidation of cyclopentene to glutaraldehyde. *J. Mol. Catal. A Chem.* **2005**, *241*, 205–214. [[CrossRef](#)]
33. Zhao, D.; Rodriguez, A.; Dimitrijevic, N.M.; Rajh, T.; Koodali, R.T. Synthesis, structural characterization, and photocatalytic performance of mesoporous W-MCM-48. *J. Phys. Chem. C* **2010**, *114*, 15728–15734. [[CrossRef](#)]



34. Dimitrov, L.; Palcheva, R.; Spojakina, A.; Jiratova, K. Synthesis and characterization of W-SBA-15 and W-HMS as supports for HDS. *J. Porous Mater.* **2011**, *18*, 425–434. [[CrossRef](#)]
35. Yang, X.-L.; Dai, W.-L.; Chen, H.; Cao, Y.; Li, H.; He, H.; Fan, K. Novel efficient and green approach to the synthesis of glutaraldehyde over highly active W-doped SBA-15 catalyst. *J. Catal.* **2005**, *229*, 259–263. [[CrossRef](#)]
36. Bordoloi, A.; Vinu, A.; Halligudi, S.B. One-step synthesis of SBA-15 containing tungsten oxide nanoclusters: A chemoselective catalyst for oxidation of sulfides to sulfoxides under ambient conditions. *Chem. Commun.* **2007**, 4806–4808. [[CrossRef](#)] [[PubMed](#)]
37. Yang, X.-L.; Dai, W.-L.; Chen, H.; Xu, J.-H.; Cao, Y.; Li, H.; Fan, K. Novel tungsten-containing mesoporous HMS material: Its synthesis, characterization and catalytic application in the selective oxidation of cyclopentene to glutaraldehyde by aqueous H<sub>2</sub>O<sub>2</sub>. *Appl. Catal. A Gen.* **2005**, *283*, 1–8. [[CrossRef](#)]
38. Ke, I.-S.; Liu, S.-T. Synthesis and catalysis of tungsten oxide in hexagonal mesoporous silicas (W-HMS). *Appl. Catal. A Gen.* **2007**, *317*, 91–96. [[CrossRef](#)]
39. Gao, R.; Yanga, X.; Dai, W.-L.; Le, Y.; Li, H.; Fan, K. High-activity, single-site mesoporous WO<sub>3</sub>-MCF materials for the catalytic epoxidation of cycloocta-1,5-diene with aqueous hydrogen peroxide. *J. Catal.* **2008**, *256*, 259–267. [[CrossRef](#)]
40. Su, Y.; Liu, Y.-M.; Wang, L.-C.; Chen, M.; Cao, Y.; Dai, W.-L.; He, H.-Y.; Fan, K.-N. Tungsten-containing MCF silica as active and recyclable catalysts for liquid-phase oxidation of 1,3-butanediol to 4-hydroxy-2-butanone. *Appl. Catal. A Gen.* **2006**, *315*, 91–100. [[CrossRef](#)]
41. Ramanathan, A.; Maheswari, R.; Grady, B.P.; Moore, D.S.; Barich, D.H.; Subramaniam, B. Tungsten-incorporated cage-type mesoporous silicate: W-KIT-5. *Microporous Mesoporous Mater.* **2013**, *175*, 43–49. [[CrossRef](#)]
42. Ramanathan, A.; Subramaniam, B.; Badloe, D.; Hanefeld, U.; Maheswari, R. Direct incorporation of tungsten into ultra-large-pore three-dimensional mesoporous silicate framework: W-KIT-6. *J. Porous Mater.* **2012**, *19*, 961–968. [[CrossRef](#)]
43. Ten Dam, J.; Badloe, D.; Ramanathan, A.; Djanashvili, K.; Kapteijn, F.; Hanefeld, U. Synthesis, characterisation and catalytic performance of mesoporous tungsten silicate: W-TUD-1. *Appl. Catal. A Gen.* **2013**, *468*, 150–159. [[CrossRef](#)]
44. Pope, M.T. *Heteropoly- and Isopolyoxometalates*; Springer: Berlin, Germany, 1983.
45. Karakonstantis, L.; Kordulis, C.; Lycourghiotis, A. Mechanism of adsorption of tungstates on the interface of  $\gamma$ -alumina/electrolyte solutions. *Langmuir* **1992**, *8*, 1318–1324. [[CrossRef](#)]
46. Salles, L.; Aubry, C.; Thouvenot, R.; Robert, F.; Doremieux-Morin, C.; Chottard, G.; Ledon, H.; Jeannin, Y.; Bregeault, J.-M. <sup>31</sup>P and <sup>183</sup>W NMR spectroscopic evidence for novel peroxo species in the “H<sub>3</sub>[PW<sub>12</sub>O<sub>40</sub>] $\cdot$ yH<sub>2</sub>O/H<sub>2</sub>O<sub>2</sub>” system. Synthesis and X-ray structure of tetrabutylammonium ( $\mu$ -Hydrogen phosphato)bis( $\mu$ -peroxo)bis(oxoperoxotungstate)(2-): A catalyst of olefin epoxidation in a biphasic medium. *Inorg. Chem.* **1994**, *33*, 871–878.
47. Ivanchikova, I.D.; Kovalev, M.K.; Mel’gunov, M.S.; Shmakov, A.N.; Kholdeeva, O.A. User-friendly synthesis of highly selective and recyclable mesoporous titanium-silicate catalysts for the clean production of substituted p-benzoquinones. *Catal. Sci. Technol.* **2014**, *4*, 200–207. [[CrossRef](#)]
48. Ivanchikova, I.D.; Maksimchuk, N.V.; Skobelev, I.Y.; Kaichev, V.V.; Kholdeeva, O.A. Mesoporous niobium-silicates prepared by evaporation-induced self-assembly as catalysts for selective oxidations with aqueous H<sub>2</sub>O<sub>2</sub>. *J. Catal.* **2015**, *332*, 138–148. [[CrossRef](#)]
49. Zhu, H.; Maheswari, R.; Ramanathan, A.; Subramaniam, B. Evaporation-induced self-assembly of mesoporous zirconium silicates with tunable acidity and facile catalytic dehydration activity. *Microporous Mesoporous Mater.* **2016**, *223*, 46–52. [[CrossRef](#)]
50. Wu, J.-F.; Ramanathan, A.; Subramaniam, B. Novel tungsten-incorporated mesoporous silicates synthesized via evaporation-induced self-assembly: Enhanced metathesis performance. *J. Catal.* **2017**, *350*, 182–188. [[CrossRef](#)]
51. Ramanathan, A.; Wu, J.-F.; Maheswari, R.; Hu, Y.; Subramaniam, B. Synthesis of molybdenum-incorporated mesoporous silicates by evaporation-induced self-assembly: Insights into surface oxide species and corresponding olefin metathesis activity. *Microporous Mesoporous Mater.* **2017**, *245*, 118–125. [[CrossRef](#)]
52. Kholdeeva, O.A. Recent developments in liquid-phase selective oxidation using environmentally benign oxidants and mesoporous metal silicates. *Catal. Sci. Technol.* **2014**, *4*, 1869–1889. [[CrossRef](#)]

53. Baxter, D.V.; Chisolm, M.H.; Doherty, S.; Gruhn, N.E. Chemical vapour deposition of electrochromic tungsten oxide films employing volatile tungsten(VI) oxo alkoxide/ $\beta$ -diketonate complexes. *Chem. Commun.* **1996**, 1129–1130. [[CrossRef](#)]
54. Choujaa, H.; Johnson, A.L.; Kociok-Köhn, G.; Molloy, K.C. Synthesis of heterobimetallic tungsten acetylacetonate/alkoxide complexes and their application as molecular precursors to metal tungstates. *Polyhedron* **2013**, *59*, 85–90. [[CrossRef](#)]
55. Kustova, G.N.; Chesalov, Y.A.; Plyasova, L.M.; Molina, I.Y.; Nizovskii, A.I. Vibrational spectra of  $\text{WO}_3 \cdot n\text{H}_2\text{O}$  and  $\text{WO}_3$  polymorphs. *Vib. Spectrosc.* **2011**, *55*, 235–240. [[CrossRef](#)]
56. Graselli, J.G.; Bulkin, B.J. *Analytical Raman Spectroscopy*; Wiley: New York, NY, USA, 1991; p. 352.
57. Griffith, W.P.; Wickins, T.D. Raman studies on species in aqueous solutions. Part II. Oxy-species of metals of Groups VIA, VA, and IVA. *J. Chem. Soc. A* **1967**, 675–679. [[CrossRef](#)]
58. Maćzka, M.; Hanuza, J.; Waśkowska, A. Vibrational studies of alkali metal hexatungstates. *J. Raman Spectrosc.* **2003**, *34*, 432–437. [[CrossRef](#)]
59. Ivanchikova, I.D.; Skobelev, I.Y.; Maksimchuk, N.V.; Paukshtis, E.A.; Shashkov, M.V.; Kholdeeva, O.A. Toward understanding the unusual reactivity of mesoporous niobium silicates in epoxidation of C=C bonds with hydrogen peroxide. *J. Catal.* **2017**, *356*, 85–99. [[CrossRef](#)]
60. Maurya, M.R.; Kumar, M.; Sikarwar, S. Polymer-anchored oxoperoxo complexes of vanadium(V), molybdenum(VI) and tungsten(VI) as catalyst for the oxidation of phenol and styrene using hydrogen peroxide as oxidant. *React. Funct. Polym.* **2006**, *66*, 808–818. [[CrossRef](#)]
61. Adam, F.; Iqbal, A. The liquid phase oxidation of styrene with tungsten modified silica as a catalyst. *Chem. Eng. J.* **2011**, *171*, 1379–1386. [[CrossRef](#)]
62. Sheldon, R.A.; Wallau, M.; Arends, I.W.C.E.; Schuchardt, U. Heterogeneous Catalysts for Liquid-Phase Oxidations: Philosophers' Stones or Trojan Horses? *Acc. Chem. Res.* **1998**, *31*, 485–493. [[CrossRef](#)]
63. Adachi, K.; Toyomura, S.; Miyakuni, Y.; Yamazaki, S.; Honda, K.; Hirano, T. Dioxomolybdenum(VI) and dioxotungsten(VI) complexes: Efficient catalytic activity for crosslinking reaction in ethylene-vinyl acetate copolymer/alkoxysilane composites. *Polym. Adv. Technol.* **2015**, *26*, 597–605. [[CrossRef](#)]
64. Buono-Core, G.E.; Klahn, A.H.; Castillo, C.; Bustamante, M.J.; Munoz, E.; Cabello, G.; Chornik, B. Synthesis and evaluation of bis- $\beta$ -diketonate dioxotungsten(VI) complexes as precursors for the photodeposition of  $\text{WO}_3$  films. *Polyhedron* **2011**, *30*, 201–206. [[CrossRef](#)]
65. Yu, S.; Holm, R.H. Aspects of the oxygen atom transfer chemistry of tungsten. *Inorg. Chem.* **1989**, *28*, 4385–4391. [[CrossRef](#)]



© 2018 by the authors. Licensee MDPI, Basel, Switzerland. This article is an open access article distributed under the terms and conditions of the Creative Commons Attribution (CC BY) license (<http://creativecommons.org/licenses/by/4.0/>).